# *Bis*(terpyridine)-based surface template structures on graphite: a force field and DFT study

Daniela Künzel, Thomas Markert, and Axel Groß
*Institut für Theoretische Chemie, Universität Ulm, D-89069 Ulm, Germany*

David M. Benoit
*Nachwuchsgruppe Theorie - SFB 569, Universität Ulm, D-89069 Ulm, Germany*

Host-guest networks formed by ordered organic layers are promising candidates for applications in molecular storage and quantum computing. We have studied 2-dimensionally ordered surface template structures of bis(terpyridine)-derived molecules (BTPs) on graphite using force field and DFT methods and compared the results to recent experimental observations. In order to determine the force field best suited for surface calculations, bond lengths and angles, torsional potentials, adsorption and stacking energies of smaller aromatic molecules were calculated with different force fields (Compass, UFF, Dreiding and CVFF). Density functional perturbation theory calculations were used to study the intermolecular interactions between 3,3'-BTP molecules. Structural properties, adsorption energies and rotational barriers of the 3,3'-BTP surface structure and its host-guest systems with phthalocyanine ($PcH_2$) or excess 3,3'-BTP as guest molecules have been addressed. In addition, STM images of oligopyridine and phthalocyanine molecules were simulated based on periodic and local density functional theory calculations.

## I. INTRODUCTION

Two-dimensional networks of organic molecules have attracted growing interest in recent years as potential new materials for sensing, catalysis, molecular electronics [1–3]. These networks can also form host-guest structures which are promising candidates for applications in molecular storage and quantum computing [4, 5]. In particular, oligopyridines such as bis(terpyridine)-derived molecules (BTPs, see Fig. 1a) have been studied recently on account of their versatility as building blocks for self-assembled nanostructures [6, 7]. Generally, the formation of such ordered surface structures has been attributed to weak intermolecular interactions between adsorbed molecules. Molecules capable of forming hydrogen bonds are favored for this purpose, as this kind of bonding is both directed and selective.

In the case of the pyridine-based molecules, intermolecular interactions occur in the form of weak C-H$\cdots$N bonds, which should determine both the prevailing conformational isomer of the molecule and the surface structure that can be created from it. On graphite surfaces, a coplanar arrangement of oligopyridine molecules mediated through $\pi$-$\pi$-interactions is usually assumed [8]. Depending on the constitutional isomer of the oligopyridine molecule and on experimental conditions such as solvent and concentration, various structures could be observed on graphite in STM experiments [6, 8]. Among these, a low-concentration structure of 3,3'-BTP with large hexagonal cavities is of special interest because the cavities can be used as a template for further adsorption of phthalocyanine ($PcH_2$) and copper phthalocyanine (CuPc, Fig. 1b) and excess 3,3'-BTP, [4] thus providing a possibility to include metal centers in form of complexes in the ordered structure. However, the fourfold symmetry of the phthalocyanine complex could not be observed in these experimental STM images, so a rotational motion of the molecule within the cavities was assumed.

Concerning electronic structure calculations of the oligopyridine surface structures, the size of the system is the main setback: calculations of surface structures consisting of unit cells with several hundreds of atoms still represent a significant computational challenge within standard density functional theory (DFT) methods. As an alternative, the combination of DFT methods with classical force fields might be a promising approach to study the structure formation of extended organic layers [9]. Yet most available force fields are optimized for the study of organic polymers or molecules of biological interest such as proteins. Using force fields for the calculation of complex surface structures still seems to be rather exceptional. To the best of our knowledge, reports on adsorption energies obtained from molecular mechanics methods are rather scarce. This shows that force fields are not yet commonly used for surface and adsorption problems in spite of their efficiency and sug-

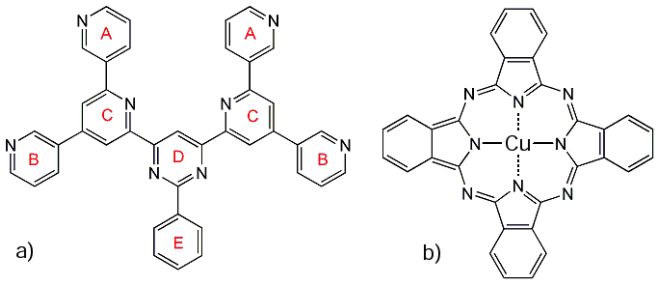


FIG. 1: Structures of a) *bis*(terpyridine) derivative 3,3'-BTP and of b) copper phthalocyanine (CuPc)

gests the need of a study concerning their applicability for these kinds of questions.

In this paper, motivated by recent STM experiments [4–6], we address *bis*(terpyridine)-based surface template structures on graphite by a combination of different force field and DFT methods in order to gain insight into the principles responsible for the structure formation in such systems. At the same time, in order to assess the reliability of various force field parameterizations with respect to adsorption problems, we compare the results of different force fields in detail with existing experimental and first-principles results. In addition, we simulate STM images of oligopyridine and phthalocyanine molecules as an aid for the interpretation of STM images.

## II. COMPUTATIONAL DETAILS

### 1. Force field calculations

In this study, a combination of force field and DFT methods is used in order to address BTP-based ordered structures on graphite. Surface structures, adsorption energies and rotational barriers are calculated with force field methods. We use the Universal (UFF), [10] Compass (condensed-phase optimized molecular potentials for atomistic simulation studies), [11] Dreiding [12] and Consistent Valence (CVFF) [13] force fields included in the Forcite module of the Accelrys' Materials Studio package. The graphite surface is modeled by a graphite (0001) slab, the atomic positions of the lower carbon layers are kept fixed after initial optimization of the graphite structure. Convergence criteria are chosen according to the program's fine and ultrafine settings which corresponds to a convergence of the energies of better than $1\times10^{-4}$ and $2\times10^{-5}$ kcal/mol, respectively, and of the residual forces of better than $5\times10^{-3}$ and $1\times10^{-3}$ (kcal/mol)/Å, respectively.

Partial charges of the atoms are assigned with the Gasteiger method for UFF and Dreiding, [14] whereas charging methods are already included in the CVFF and Compass force fields. Adsorption energies ($E_{ads}$) are calculated by comparing the total energy of the surface structures ($E_{tot}$) to the energies of the clean graphite surface ($E_{surf}$) and the adsorbate molecule(s) optimized in the gas phase ($E_{gas}$).

$$E_{ads} = E_{tot} - (E_{surf} + E_{gas}) \quad (1)$$

To compute the rotational barrier of phthalocyanine in a hexagonal cavity, we use only a one-layer graphite slab with fixed atomic positions in order to reduce computational cost. The molecule is rotated stepwise in the cavity, the resulting structure is optimized with medium convergence criteria. To prevent the phthalocyanine molecule from moving back to its original position, its nitrogen atoms are kept fixed during the optimization process.

### 2. Density functional theory calculations

DFT methods have been used for two purposes: first, to determine the nature of the interaction between the BTP molecules within density functional perturbation theory (DFPT), and second, to determine molecular properties and to simulate STM images.

The DFPT calculations have been carried out using the CPMD ab initio pseudopotential plane-wave package [15] along with the gradient-corrected Perdew-Burke-Ernzerhof (PBE) exchange and correlation functional [16]. This particular functional has been shown to provide a good description of weak hydrogen bonds [17]. The initial rectangular unit cell describing the monolayer is derived from the experimental STM estimations of Meier *et al.* [6]. In every case, the inter-layer distance is kept to 16 Å. The geometry optimizations are performed with Vanderbilt ultra-soft pseudo potentials [18] and a plane-wave cut-off energy of 30 Ry. The optimizations use a linearly scaling BFGS algorithm [19] and are terminated when the largest atomic gradient component was below $5 \cdot 10^{-4}$ H/bohrs. For each optimized geometry, density functional perturbation theory calculations are performed using a parallel implementation of the method described in Ref. [20], Goedecker norm-conserving pseudo potentials, [21, 22] and a plane-wave cut-off energy of 100 Ry. All DFPT calculations were performed on a cluster of Apple X-Serve computers.

STM images have been simulated based on both local as well as periodic DFT calculations in order to enable a comparison with experiments [6, 23, 24]. Geometry optimizations of the organic molecules involved are carried out with the Gaussian 03 program [25] using the B3LYP exchange-correlation potential [26] and various basis sets (see text below). To reduce the computational cost, phthalocyanines are optimized under the constraints of $D_{2h}$ and $D_{4h}$ symmetry. In addition, periodic DFT calculations have been performed using the Vienna *ab initio* Simulation Package (VASP) [27] and the PBE functional [16]. The ionic cores were represented by projected augmented wave (PAW) potentials [28, 29]. The Kohn-Sham states were expanded in a plane wave basis with an energy cut-off of 30 Ry. For the **k**-point summation over the first Brillouin zone, only the Gamma point was used.

Using VASP, we also determined the electronic structure of molecules on a graphene layer based on UFF geometries in order to assess the influence of the graphite surface on STM images. The STM simulations are based on the Tersoff-Hamann picture [30] in which the tunneling current is simply proportional to the local density of states at the surface close to the Fermi energy at the position of the tip. Depending on the corresponding bias, occupied and unoccupied electronic states of the oligopyridine and phthalocyanine molecules with and without graphene have been taken into account within a small energy range.

TABLE I: Average bond lengths and angles in 2,2'- and 4,4'-bipyridine calculated with DFT (B3LYP/TZVP) and force field methods (angles in degrees, lengths in Å)

| | 2,2'-bipyridine [31] | | | | | 4,4'-bipyridine | | | | |
|---|---|---|---|---|---|---|---|---|---|---|
| | C-C (av.) | C-N (av.) | C-N-C | $N_1$-$C_6$-$C_5$ | $C_2$-$C_{2'}$ | C-C (av.) | C-N (av.) | C-N-C | $C_4$-$C_{4'}$ | $C_3$-$C_4$-$C_{4'}$-$C_{3'}$ |
| exp. | 1.389(2) | 1.352(4) | 116.2(7) | 124.6(6) | 1.496(3) | 1.393[32][a] | 1.338[32][a] | 116.9[32][a] | 1.470 [33] | 37.2 [33] |
| Compass | 1.396 | 1.351 | 116.8 | 123.7 | 1.445 | 1.399 | 1.341 | 118.3 | 1.442 | 24.4 |
| Dreiding | 1.409 | 1.350 | 124.3 | 119.5 | 1.416 | 1.412 | 1.356 | 122.4 | 1.414 | 47.5 |
| UFF | 1.399 | 1.362 | 122.2 | 120.0 | 1.485 | 1.401 | 1.359 | 121.6 | 1.485 | 40.5 |
| CVFF | 1.404 | 1.347 | 123.2 | 120.9 | 1.418 | 1.414 | 1.326 | 121.0 | 1.417 | 16.9 |
| B3LYP | 1.392 | 1.336 | 118.4 | 123.5 | 1.489 | 1.393 | 1.334 | 116.9 | 1.481 | 38.8 |

[a]Experimental values for pyridine (gas-phase microwave spectra)

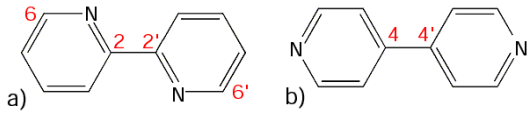


FIG. 2: Structures of a) 2,2'- and b) 4,4'-bipyridine

## III. RESULTS

### A. Comparison of force fields

The suitability of different force fields for the calculation of structural and energetic surface properties has to be discussed in order to determine the one(s) best suited for surface structure and adsorption energy calculations. We thus calculate bond lengths and angles, torsional properties and adsorption energies and then compare our force field results to the corresponding experimental data.

Due to the availability of experimental data, 2,2'- and 4,4'-bipyridine (Fig. 2) are used as models for geometric properties and torsional barriers and a number of small aromatic molecules are used to study adsorption energies on graphite. The stacking energy of a pyridine-benzene dimer is calculated as a model for the substrate-adsorbate interaction in our system.

#### 1. *Bond lengths and bond angles of bipyridines*

The force field reproduction of aromatic bond lengths and bond angles is reasonably accurate with all methods (Table I): Compared to experimental results, average aromatic C-C bonds in 2,2'-bipyridine are overestimated by up to 2%. In 4,4'-bipyridine, they are underestimated by less than 1.5%. Aromatic C-N bonds are within 1.6% of experiment for both molecules. Calculation of bond angles is less accurate, a deviation from experimental data up to 7% can be observed for some extreme cases such as the C-N-C angle in 4,4'-bipyridine. However, typically this deviation is around 2-3%, which is only slightly larger than the value obtained for bond lengths. The best agreement with respect to experimental data can be found for Compass and UFF.

Reported errors for the UFF force field [10] are less than 0.1 Å in bond lengths and of 5-10° in angle bends. The errors were determined with a validation set containing various small organic, main group inorganic and organometallic molecules. Dreiding had an rms error of 0.035 Å for bond lengths, 3.2° for angles and 8.9° for torsions in a set of 76 organic molecules. [12] In a set of isolated organic molecules, Compass shows an rms deviation of 0.9% for bond lengths and 1.8% for angles. However, the Compass functional form for valence bonds is less suitable for the description of biarylic compounds and other molecules with unusual bond orders, because those are currently not fully taken into account. [11] If we use for our calculations the error range obtained from the force field validation, we can see that for Dreiding and some of the Compass data, the experimental values are outside the error range of the force field. Yet for the UFF and the rest of the Compass calculations the experimental data is within the error margin of the calculations.

For an accurate description of the oligopyridine structure, not only aromatic bonds and angles but also the C-C single bond and torsion angle between aromatic rings should be reproduced correctly. Since force field results vary greatly, these properties are the most obvious criteria to determine the applicability of a force field for the calculation of oligopyridine structural properties.

In agreement with experimental results, UFF describes the C-C single bond between pyridine rings as slightly shortened aliphatic single bond. However, Dreiding, Compass and CVFF calculations result in a bond length comparable to an elongated aromatic C-C bond. Due to steric repulsion of hydrogen atoms and the formation of weak C-H$\cdots$N hydrogen bonds, 2,2'-bipyridine has a stable conformation with a transoid arrangement of the nitrogen atoms. [31] This conformation can be reproduced with all force fields apart from Compass which favors a cisoid arrangement over a nearly transoid one by 30.56 kJ/mol. For 4,4'-bipyridine, torsion angles calculated with CVFF and Compass are too small, whereas with Dreiding they are clearly overestimated. The best

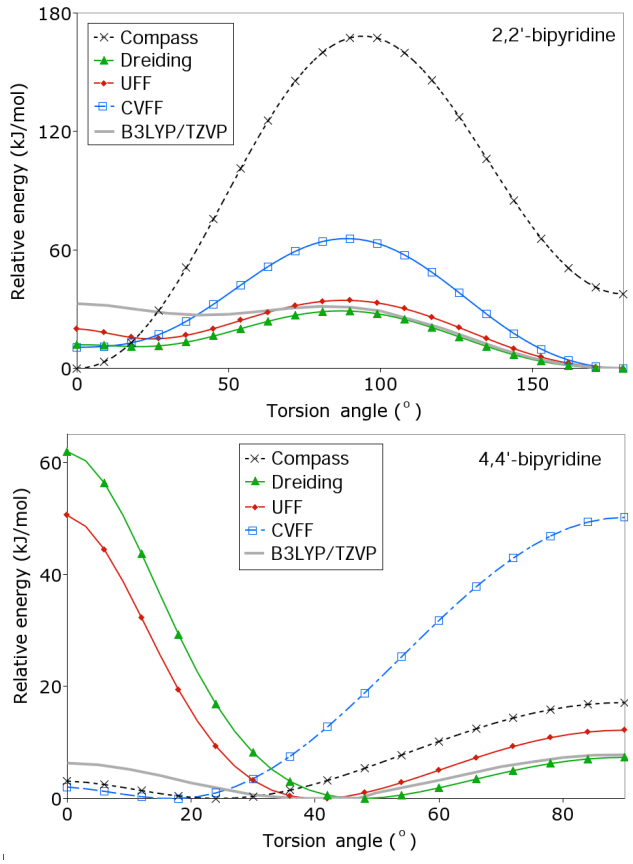


FIG. 3: Torsional potential energy curves of 2,2'- and 4,4'-bipyridine in kJ/mol with respect to minimum energy

result is obtained with the Universal force field, whose torsion angles are similar to DFT and experimental results.

### 2. *Rotation around C-C single bonds in bipyridines*

As the discrepancies of torsion angles in optimized geometries might also be explained by a flat potential energy surface with several local minima, we now examine the torsional potentials. The torsion angle in previously optimized bipyridines is changed stepwise and the absolute energy of the resulting conformation is calculated.

Potential energy curves for UFF and Dreiding are very similar, with minima at nearly the same positions and comparable barrier heights. Compass and CVFF show a completely different behavior for both molecules (Fig. 3).

In most cases, the optimum conformation for 2,2'-bipyridine is the N-N-transoid arrangement that was also obtained from a simple geometry optimization. Only Compass favors the cisoid arrangement. All force fields find a maximum in energy at 90°, but the description of the N-N cisoid conformation shows great discrepancies between force fields. Whereas this conformation is the absolute minimum with Compass and a local minimum

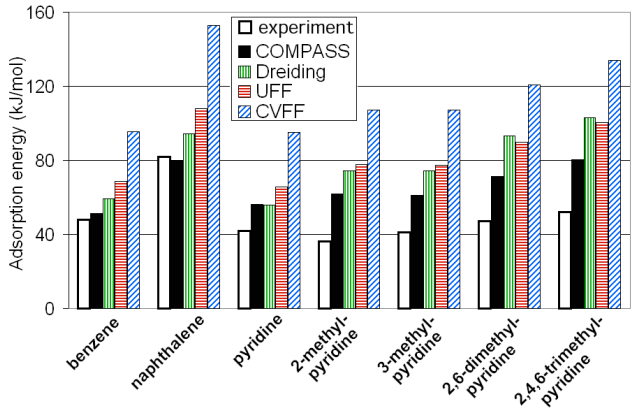


FIG. 4: Adsorption energies of small aromatic molecules on graphite, experimental and force field data in kJ/mol with respect to the free molecules.

with CVFF, it represents a local maximum in UFF and Dreiding calculations, with local minima appearing at 33° (UFF) and 30°(Dreiding). Our DFT calculations carried out with B3LYP/TZVP [34] (calculated with Gaussian 03) result in a curve progression similar to the UFF and Dreiding results, with a less pronounced local minimum at 40°.

The rotational barrier is highest with the Compass force field (162.5 kJ/mol), CVFF yields a barrier of 63.2 kJ/mol. The results for UFF and Dreiding are very similar with 33.8 and 28.6 kJ/mol. There also is a good agreement with the 32.8 kJ/mol obtained using DFT. Previous calculations resulted in a difference of 35.3 (MP2) and 32.0 kJ/mol (DFT/B3LYP) between transoid and cisoid conformation and in a shape of the potential energy curve matching our results. [35]

4,4'-Bipyridine has a single minimum between 20° and 50°, depending on the force field, which was also located in the geometry optimizations mentioned above. As there is only one minimum, we can rule out the possibility of different force fields favoring different local minima, the differences in optimized torsion angles must be attributed to the inherent characteristics of the force fields.

The torsion angle corresponding to the energetic minimum differs from force field to force field. Moreover, the barrier heights of 4,4'-bipyridine also show a significant variation. Both UFF and CVFF yield very similar values of 50.6 and 50.1 kJ/mol as the highest energy difference possible in this system. The main difference is the position of the absolute maximum, which is at 0° for UFF and at 90° for CVFF. The rotational barrier obtained from Dreiding is even higher (61.9 kJ/mol), the absolute maximum can again be found at 0°. Compass shows the same behavior as CVFF with a rather low barrier of only 16.4 kJ/mol. The Compass potential energy curve is similar in shape to the DFT (B3LYP/TZVP) results, but with only 7.8 kJ/mol the DFT barrier is lower. The results are comparable to those of previous DFT and

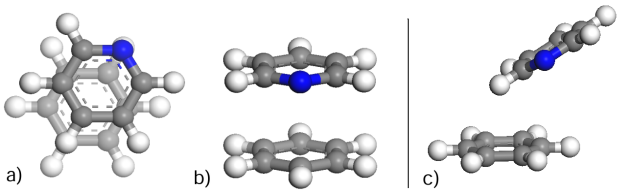


FIG. 5: Parallel-displaced mixed pyridine/benzene dimer, a) top view and b) side view calculated with UFF, c) side view calculated with Compass

MP2 calculations with a barrier of 8.4-9.2 kJ/mol and an absolute maximum at 90°. [36]

### 3. *Adsorption of small aromatic molecules on graphite*

Fine convergence criteria are used for the optimization of simple aromatic molecules adsorbed on a 2-layer graphite slab, with the lower layer kept fixed. A 3-layer graphite slab and ultrafine convergence criteria are used for phthalocyanine and 3,3'-BTP in order to be consistent with subsequent surface optimizations. Adsorption energies are determined according to the procedure mentioned in section II.

Both calculated and experimental adsorption energies on graphite increase with the size of the adsorbed aromatic molecule. This supports the assumption of $\pi$-$\pi$-interactions between the aromatic adsorbate and the graphite surface that has previously been used to explain the planar arrangement of oligopyridines on the surface. [8]

Apart from naphthalene calculated with Compass, experimentally determined gas-phase adsorption data shows that force field adsorption energies are generally overestimated. However, results vary strongly with the force field used. For nearly all the chosen molecules, adsorption energies follow the same general trend: Adsorption energies are smallest when calculated with Compass. Next follow Dreiding and UFF, with higher energies for UFF in most but not all cases (Fig. 4).

CVFF yields the highest adsorption energies, calculated values are 2-3 times higher than corresponding experimental ones, the average scaling factor is 2.4 (Table II). The same effect can be observed for the UFF and Dreiding force fields, where average calculated adsorption energies are 1.6 and 1.7 times too high. The best agreement could be obtained with the Compass force field. With the exception of naphthalene, values are 1.1 to 1.7 times higher than experimental values, with an average of 1.35. These values could be used to roughly estimate adsorption energies from force field results.

TABLE II: Adsorption energies of aromatic molecules on graphite (kJ/mol), experimental and force field data

| | exp. | Compass | UFF | CVFF | Dreiding |
|---|---|---|---|---|---|
| benzene | 48 [37] | 51.19 | 68.59 | 95.48 | 59.25 |
| naphthalene | 82 [37] | 79.59 | 107.82 | 152.58 | 94.20 |
| coronene | 135 [37] | 180.87 | 235.87 | 345.33 | 210.01 |
| ovalene | 203 [37] | 237.05 | 308.01 | 454.08 | 275.43 |
| pyridine | 41.8 [38] | 56.33 | 65.66 | 94.93 | 55.97 |
| 2-methyl-pyridine | 36.4 [38] | 61.81 | 77.88 | 107.13 | 74.28 |
| 3-methyl-pyridine | 41.3 [38] | 61.18 | 77.5 | 107.02 | 74.28 |
| 2,6-dimethyl-pyridine | 47.1 [38] | 71.18 | 89.73 | 120.65 | 93.27 |
| 2,4,6-trimethyl-pyridine | 52.1 [38] | 80.55 | 100.33 | 134.09 | 102.94 |
| phthalocyanine | — | 319.22 | 390.45 | 573.7 | 338.42 |
| 3,3'-BTP | — | 391.48 | 442.61 | 708.55 | 368.55 |

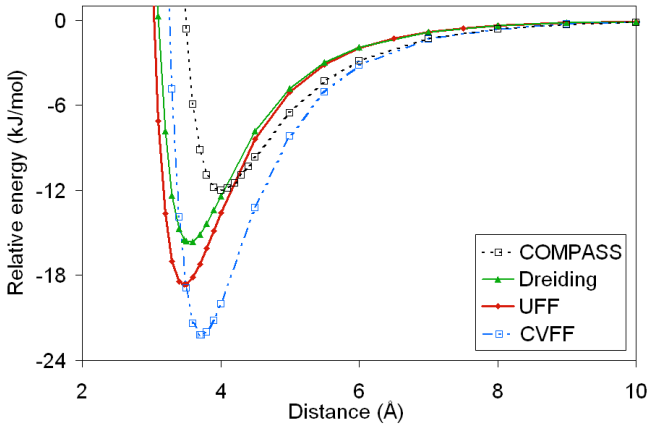


FIG. 6: Interaction energy of a parallel-displaced pyridine/benzene dimer (kJ/mol), taken with respect to both molecules 15 Å apart from each other.

### 4. *Stacking interaction*

A parallel-displaced mixed pyridine/benzene dimer (Fig. 5) can be used to model the van der Waals interaction between oligopyridine molecules and the graphite surface. Previous MP2/6-31G(0.25)* calculations had resulted in an interaction energy of 11.64 kJ/mol with a pyridine-benzene-distance of 3.52 Å [39].

Compared to the MP2 data, most force fields tend to overestimate energies or equilibrium distances which is interesting to note since MP2 is known to usually overestimate weak dispersive interactions.

The intermolecular distance (3.47 Å) obtained with UFF and Dreiding is close to the MP2 value, but interaction energies (18.67 and 15.46 kJ/mol) are too high. With an equilibrium distance of 3.72 Å and a stacking energy of 22.23 kJ/mol, CVFF overestimates both properties (Fig. 6).

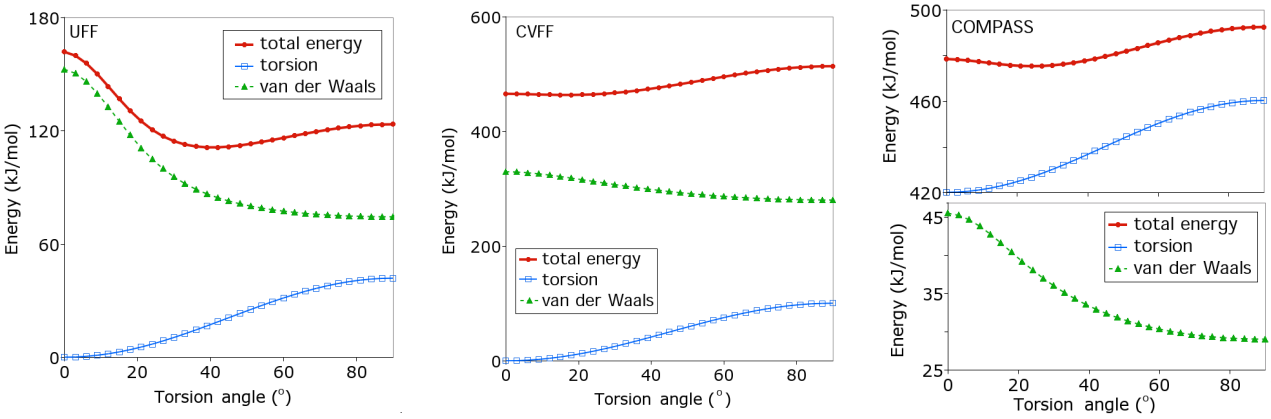


FIG. 7: Torsional potential energy curves of 4,4'-bipyridine with UFF, CVFF and Compass, split into single contributions

The best agreement in interaction energy can be obtained from Compass calculations, the value of 12.03 kJ/mol is only 3.4 % higher than the MP2 result. However, the potential energy curve is based on the optimized geometry obtained with Compass. In contrast to the flat geometry of adsorbates on graphite, the optimized dimer is not planar any more. The pyridine is tilted by approximately 30° in relation to the benzene plane. Thus the intermolecular distance varies between 2.93 and 5.11 Å, the average distance is 4.00 Å.

#### 5. *Summary: Suitability of force fields*

The comparison of force fields yields different results depending on the problem investigated: Geometric properties of simple aromatic systems are described adequately by all force fields, but when it comes to the more complex torsion angles and biarylic C-C single bonds, the best result can be obtained with UFF, which was developed with the objective of accurate structure predictions for a broad range of elements and bonding situations.

The results for the bipyridine torsional potentials prove to be inconsistent. UFF and Dreiding provide the best description for 2,2-bipyridine, whereas the 4,4'-bipyridine torsional DFT potential is most closely reproduced by Compass. In order to understand the discrepancies between the different force fields, we analyzed the different contributions to the total energy. In principle, a force field should be considered as a single entity [40]: the way force fields decompose the total energy into separate contributions is not unique. Still it is instructive to take a closer look at the single terms.

According to this analysis, the discrepancies are mainly due to the different behavior of van der Waals and torsional terms in each force field (see Fig. 7). In UFF and Dreiding, these terms are very similar and thus yield similar results: the van der Waals term outweighs the torsional contribution and thus dominates the torsional potential energy curve. This might be due to the fact that only atoms that are connected to each other or to a common atom are excluded from the calculation of van der Waals interactions. For CVFF, the van der Waals term is also higher than the torsional term but less steep than for UFF and Dreiding. This results in a total energy curve with a local minimum at 0° for 2,2'-bipyridine and in a rather small torsion angle for 4,4'-bipyridine. The Compass functional form differs from the others: the torsional contribution in COMPASS outweighs the van der Waals term. This difference can be explained by the use of a Lennard-Jones 9-6 function for the van der Waals interaction and by the parameterization of non-bonded parameters. [11]

Adsorption energies of aromatic molecules on graphite in a planar geometry should also be calculated with Compass. Its van der Waals contribution is smaller than in the other force fields, so it overestimates adsorption energies less.

The biggest drawback of Compass is its abovementioned inability to calculate correctly torsion angles and biarylic C-C single bond lengths in spite of the very accurate results for all other geometric properties investigated.

### B. Oligopyridine surface structures

#### 1. *General aspects of the hexagonal 3,3'-BTP surface structure*

The theoretical determination of extended ordered adsorbate structures on substrates requires periodic calculations. Therefore, as a first step a suitable supercell has to be chosen which corresponds to finding commensurate lattice vectors for the graphite surface and the oligopyridine layer structure. The STM results of the oligopyridine surface structure indicate a hexagonal unit cell with a lattice constant of about 44.7 Å [6]. The experimental value lies between the 18×18 and the 19×19 graphite supercell obtained from force fields. Calculated structures have lattice constants of about 46.0-46.8 Å for the 19×19 cell. Although the cell parameter of a 18×18 sur-

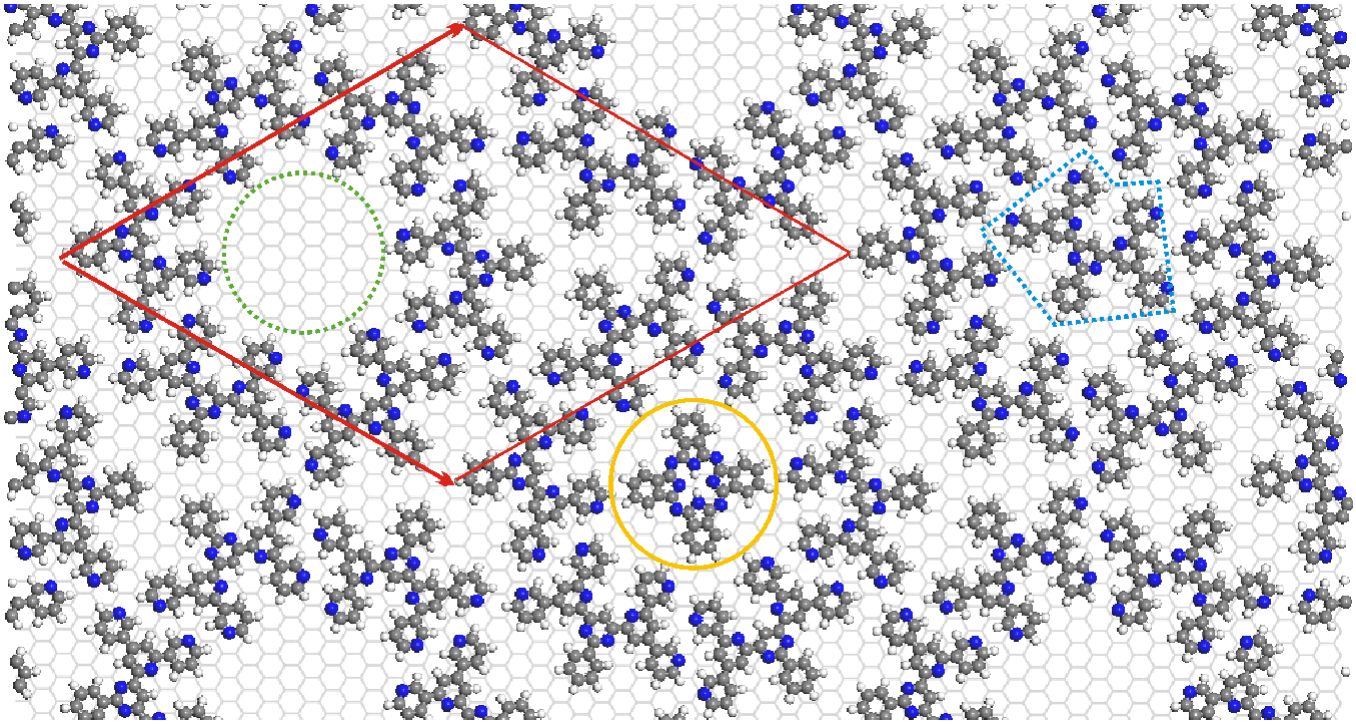

FIG. 8: Optimized template structure of 3,3'-BTP: unit cell (red arrows), hexagonal cavity (green dashed circle); with guest molecules 3,3'-BTP (dashed blue irregular shape) and phthalocyanine (yellow circle)

face unit cell (43.5-44.3 Å) is closer to the experimentally determined result, the gain in adsorption energy for the 19×19 structure is higher by 2.1-8.0 kJ/mol per molecule, depending on the choice of force field. It is also energetically more favorable than the sterically less hindered 20×20 superstructure, again there are 2.9-8.1 kJ/mol to be gained. As the 19×19 superstructure is energetically favored, further calculations have been restricted to this optimum structure, shown in Fig. 8.

Contrary to the assumption of a coplanar arrangement of the aromatic pyridine rings and the graphite surface, adsorbed molecules are not always completely planar. Conformations obtained with the CVFF and Compass force fields which underestimate bipyridine torsion angles deviate only slightly from planarity, whereas UFF and Dreiding clearly favor non-planar structures. However, the influence of $\pi$-$\pi$-interactions and steric repulsion is sufficient to diminish torsion angles from the stable gas-phase conformations. UFF calculations, which seem to be most reliable for torsion angles show a decrease of the torsion angle between aromatic rings B and C from 41° in the gas phase to 22-24° on the surface. Between rings A and C, the torsion angle also diminishes from 27-28° to a nearly planar conformation with a torsion angle of less than 5°. The other aromatic rings maintain their nearly planar arrangement both in the gas phase and on the surface.

TABLE III: Force field results for the 3,3'-BTP surface template structure: lattice constant (Å), adsorption energy $E_{ads}$ and rotational barrier (kJ/mol)

| | Compass | UFF | CVFF | Dreiding |
|---|---|---|---|---|
| $E_{ads}$ per molecule | | | | |
| 3,3'-BTP, template | 427.7 | 473.4 | 750.5 | 392.3 |
| 3,3'-BTP, guest | 416.3 | 468.0 | 797.5 | 387.9 |
| $PcH_2$, guest | 330.2 | 404.4 | 615.4 | 359.6 |
| lattice constant | 45.96 | 46.41 | 46.78 | 46.64 |
| rot. barrier | 30.3 | 56.9 | 45.7 | 39.5 |

### 2. *Nature of the interactions between 3,3'-BTP molecules*

In order to investigate in more details the nature of the interactions between 3,3'-BTP molecules in the monolayer, we performed a series of density-functional perturbation theory (DFPT) calculations of the interaction energy. This approach enables us to compute the change in electronic density generated in one molecule in response to the presence of another without making any assumptions about the nature of the interactions in the system. Moreover, this methodology has been shown to give an accurate estimation of the interaction energy for the water dimer, crystalline silicon [20], and molecular crystals [41], and does not suffer from basis-set superposition error since it uses a volumetric plane-wave basis.

We consider three possible situations: A closed-packed structure obtained from experimental STM images [6], which assumes that all 3,3'-BTP are planar (enforced using a planar constraint) and occupy a rectangular unit cell of $27 \times 16$ Å$^2$ (situation **1** in Fig. 9); an optimized structure, where all 3,3'-BTP molecules are free to relax within a rectangular $27 \times 16$ Å$^2$ unit cell (situation **2**); and finally a fully relaxed structure obtained with a larger rectangular unit cell of $29.65 \times 17.57$ Å$^2$ (situation **3**). Each unit cell contains two 3,3'-BTP molecules and, in order to limit the computational effort, the graphite layer is omitted since it is expected to contribute very little to the molecular interactions within the 3,3'-BTP monolayer.

The results of our interaction energy calculations are shown in Table IV and three response density iso-surfaces are included in Fig. 9.

For arrangement **1**, we observe that the planar geometry inferred from the experimental STM images leads to a strongly repulsive interaction between the molecules. The response density plot (see panel 1 of Fig. 9) reveals that each 3,3'-BTP molecule forms 8 weak hydrogen bonds with its neighbours between rings A and B, but also highlights the presence of close contacts between each B rings of adjacent molecules. A closer examination of the isosurface plot shows that the electron density is depleted in the lone-pair region of the nitrogen atoms and increased in the C–H$\cdots$N bond forming region, which is a clear signature of hydrogen bonds between A and B rings. We also notice that the presence of an increased electron density close to the hydrogen atom of the C–H bond induces a density shift, characteristic of an induced dipole resulting from hydrogen-bond formation. The B–B rings interactions, on the other hand, do not display the same alternating density pattern but rather show a very diffuse accumulation of electron density between the hydrogen atoms, suggesting strong undirected repulsive interactions, which overshadow completely the weak C–H$\cdots$N bonds.

When the planarity constraint of the layer is relaxed in situation **2**, the B rings twist out of the molecular plane and we observe the formation of a large number of weak C–H$\cdots$N hydrogen bonds (see panel 2 of Fig. 9). The computed strength of the interaction in this situation is remarkable but stems from the fact that each molecule can now interact with its neighbours using rings A, B, C, and E. Indeed each 3,3'-BTP unit makes up to 12 direct or bifurcated weak hydrogen bonds with an average strength of 3.25 kJ/mol. This is in line with the expected strength of the C–H$\cdots$N, given that the CCSD(T) estimates of Hartmann *et al.* [42] predict an interaction energy of 4.9 kJ/mol for the ethylene–ammonia complex.

It is interesting to consider the case of a larger unit cell, where we would expect the 3,3'-BTP molecules to adopt a more planar geometry, and display stronger intermolecular interactions, since the unit cell has more space to accommodate the molecules. Surprisingly, the larger unit cell of situation **3** does not lead to an assembly of planar 3,3'-BTP monomers (see panel 3 of Fig. 9). In-

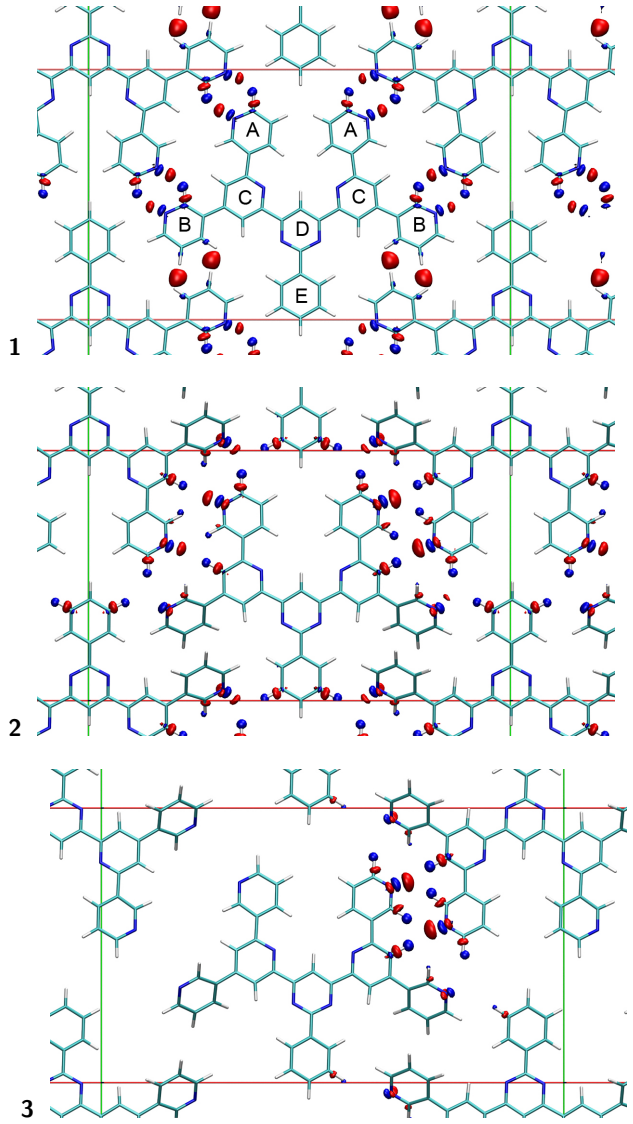


FIG. 9: Isosurface plots of the response density of isolated 3,3'-BTP monomers upon interactions within a monolayer in three different situations **1**, **2**, and **3** (see text for details). The blue zones correspond to regions where the electronic density is reduced and the red zones to regions where the density is increased, compared to the non-interacting molecules. Note that the blue and red zones enclose the same displaced charge in both cases.

TABLE IV: Computed interaction energy, $E_{\text{inter}}$, in kJ/mol per 3,3'-BTP molecules in a monolayer for various rectangular closed-packed unit cells (see text for details).

| Situation | $E_{\text{inter}}$ |
|---|---|
| **1** (exp. cell, planar) | +46.4 |
| **2** (exp. cell, relaxed) | −39.0 |
| **3** (larger cell, relaxed) | −19.4 |

stead, we observe that the B ring of each monomer is still twisted out of the molecular plane as was the case in situation **2**. This indicates that the torsion of the B ring is a property of the relaxed 3,3'-BTP monomers and is not due to a possible overcrowding occurring in the original experimental unit cell. More importantly, we note that the lower interaction energy reported in Table IV reflects a significant decrease in the number of C–H$\cdots$N hydrogen bonds in situation **3**, since the monomers are now too far apart to form hydrogen-bonded chains along the $a$ direction of the unit cell. The monomer–monomer interactions are now confined to a series of one-dimensional chains when we observed instead a true two-dimensional interaction network in situation **2**.

The experimental STM images suggested initially that the 3,3'-BTP monolayer lies flat on top of the graphite surface and that this arrangement is due to the presence of favourable C–H$\cdots$N interactions between the molecules. On the contrary, our calculations show that the free-standing monolayer is preferentially made up of non-planar 3,3'-BTP molecules and that a planar arrangement of the monomers is dominated by repulsive interactions. Interestingly, the planarity of the 3,3'-BTP is hindering the intermolecular interaction and both relaxed structures show a much stronger interaction, which highlights the importance of an accurate description of the torsion angle between rings B and C.

### *3. The 3,3'-BTP surface structure as a template for the adsorption of guest molecules*

The adsorption of another molecule of 3,3'-BTP or a molecule of phthalocyanine into the cavities of the previously formed porous 3,3'-BTP surface structure results in two different host-guest systems that could both be observed experimentally to be stable within a certain concentration range of the BTP molecules in solution. [4]

Geometric parameters of the template structure change only slightly upon addition of the guest molecule (Fig. 8). Lattice constant optimization resulted in changes of less than 2% upon addition of the guest molecule. These calculations were carried out with a 2D-periodic hexagonal arrangement of 3,3'-BTP in the gas phase under the constraint of planar molecules. Other aspects of the template structure such as dihedral angles or distance between molecules are also only marginally influenced by the presence of the guest atom.

In both cases we could observe that closer packed surface structures are energetically favored. The adsorption energy of an additional oligopyridine molecule usually is 1.1-2.6% lower than the energy gain per template molecule (Table III). Only CVFF calculations result in an adsorption energy that is 6% higher for the guest molecule. This seems to be unrealistic because it would mean that the open hexagonal structure is not thermodynamically stable against restructuring to a more dense layer, in contrast to the experimental observation [4].

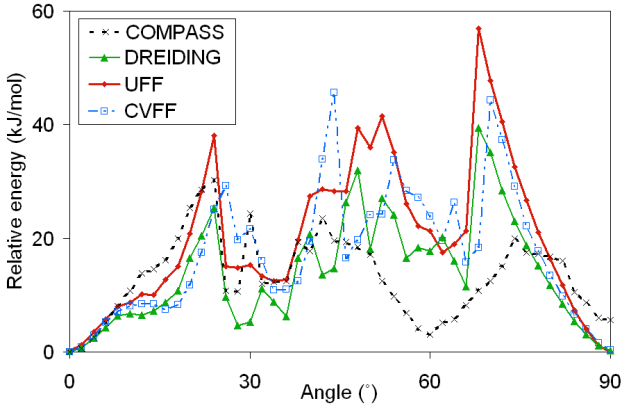


FIG. 10: Rotational potential energy curve of phthalocyanine within the cavity of the 3,3'-BTP template structure (kJ/mol), with respect to minimum energy

In the case of the smaller molecule phthalocyanine as guest molecule, the energy gain is smaller: values of only 77-92% of the adsorption energy per template molecule could be obtained. In order to understand the reasons for the stability of the porous hexagonal guest structure, we removed a single BTP molecule from the template structure and calculated the adsorption energy of this molecule with the Compass force field for the following two cases:

1. Completion of the original host structure with the BTP molecule results in a gain of 479.8 kJ/mol

2. Adsorption of the molecule in the guest position without completing the template structure only gives rise to 410.5-425.5 kJ/mol, depending on the orientation of the BTP molecule relative to the vacancy in the host network.

Even though these were mere energy calculations without further structural relaxation, these observations hint at a contribution of weak C-H$\cdots$N hydrogen bonds to the preferential formation of the hexagonal template structure.

### *4. Rotational barrier of phthalocyanine within the cavity*

The blurred STM images of the phthalocyanine molecules in the cavities [4] suggest that these molecules are immobile during the time it takes to obtain the STM images but rather rotate in the cavities of the template structure. To estimate the maximum rotational barrier, we have followed the procedure mentioned in section II: stepwise rotation followed by optimization with fixed nitrogen atoms after each step.

Starting from the optimized geometry, there are two local minima after rotation by approximately 30° and 60° (Fig. 10). The phthalocyanine molecule arrives at an

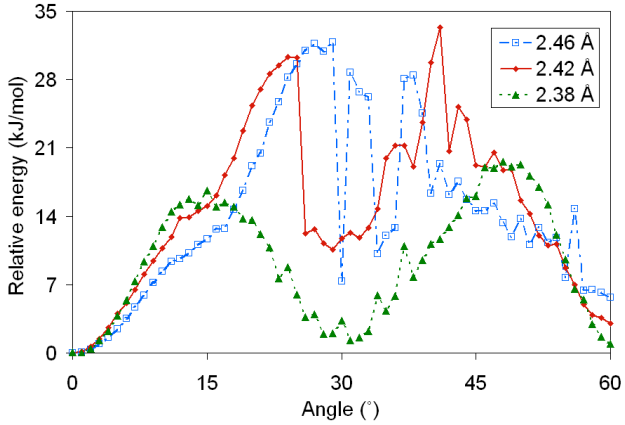


FIG. 11: Effect of changes in the graphite C-C-distance (Å) on the rotational barrier (kJ/mol), Compass calculation, energies with respect to minimum energy

arrangement similar in energy to the original state after 90°. Note that the sixfold symmetry of the cavity is not perfect due to interaction with the underlying graphite layer.

The barriers obtained are ranging from 30.3 kJ/mol for Compass to 56.9 kJ/mol for UFF. An average value of 43.1 kJ/mol can be used as approximate activation energy $E_a$ in the calculation of the rate constant $k=k_0 \cdot \exp[-E_a/k_B T]$ for the rotation. Even if the prefactor is chosen to be as low as $k_0 = 10^{10}$ $s^{-1}$, the rate constant at a temperature of 298 K is close to 300 $s^{-1}$, which enables a rotational motion that is faster than the scanning process.

The resulting potential energy curves show a strong dependence on initial atomic positions. Small changes in the starting configuration can be caused by computational specifications such as cell constant or step size and they can result in different final energies for the same rotational angle. This behavior is most pronounced at or near energetic maxima. In the course of several steps with different step sizes, the inherent imprecision of the rotational motion results in small discrepancies in atomic positions. These are sufficient for the system to find different local minima during optimization.

Small changes in the lattice constant also change initial atomic positions and thus also have an influence on phthalocyanine rotation, but not in an easily predictable way (Fig. 11). Variations of the Compass 19×19 super cell lattice constant between 45.2 and 46.7 Å (originally: 45.96 Å) show that both the shape of potential energy curve and the barrier height are affected. When the cell constant is reduced, the oligopyridine torsion angles are forced to increase. This increases the available space for the phthalocyanine rotation, so the overall shape of the energy curve changes and the barrier height decreases.

Furthermore, the presence of several local minima explains the oscillations of the energy obtained in our calculations with a step size of 1°. Rotation by small angles slightly changes starting conditions for the geometry optimization. Although all these changes are only small, their influence is sufficient to lead the system to different local minima during optimization.

TABLE V: Influence of graphite lattice constant (Å) on phthalocyanine rotational barrier height (kJ/mol), calculated with Compass

| graphite C-C-distance | lattice constant | barrier height |
|---|---|---|
| 2.38 | 46.74 | 31.80 |
| 2.40 | 46.36 | 40.45 |
| 2.42 | 45.96 | 33.35 |
| 2.44 | 45.60 | 22.89 |
| 2.46 | 45.22 | 26.86 |

### C. STM simulation

Simulation of STM images was based on DFT calculations. Both occupied and unoccupied orbitals of 3,3'-BTP and different phthalocyanines were determined with VASP and Gaussian 03 (B3LYP) using 6-311G, [43] SDD [44–46] and TZVP [34] basis sets. Experimental high-resolution STM images of copper phthalocyanine on graphite [23, 47] and copper [24] were used to identify a suitable energy range and thus the number of orbitals to use for the STM simulation. On Cu(100), copper phthalocyanine shows a fourfold symmetry, with four protrusions on each of the four main lobes [24]. Similar results of a fourfold symmetry with detailed structure can be found on graphite [23]. However, as far as the comparison of the simulated STM images with the experiment is concerned, one should note that the experimental images taken at room temperature hardly exhibit any submolecular resolution, in particular for molecules at the solid-liquid interface [4]. Only at low temperatures and ultra-high vacuum conditions, a better resolution can be achieved [48]. Therefore the theoretical results should partially be regarded as predictions.

The best agreement between calculated and experimental copper phthalocyanine images is obtained if only orbitals close to HOMO or LUMO are taken into account: The LUMO consists of two degenerate orbitals with twofold symmetry that can be combined to an STM image meeting the requirement of fourfold symmetry with four protrusions on each lobe (Fig. 12 a) – d)). Another matching image is simulated with the copper phthalocyanine HOMO which already has fourfold symmetry. If the next lower occupied orbital is also taken into account, the central part of the molecule is emphasized. Adding more orbitals changes the number and shape of protrusions (Fig. 13 a) and c)), so phthalocyanine STM simulations should be restricted to a small number of appropriate orbitals.

In the energy range chosen for the simulation of the

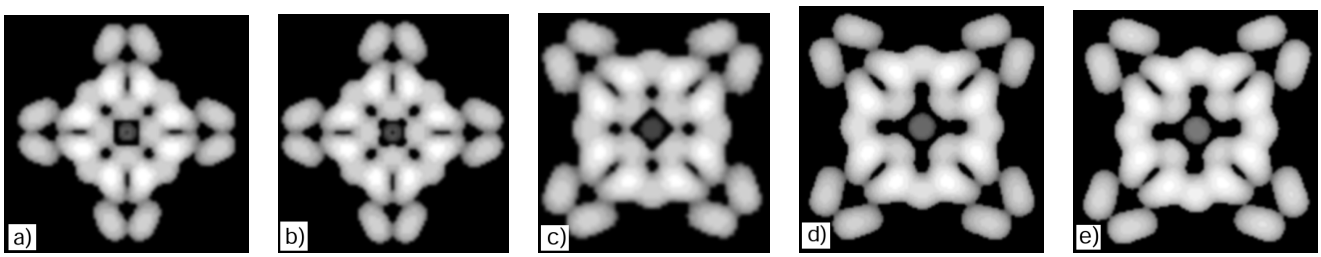


FIG. 12: Simulated STM images of the copper phthalocyanine LUMO. Gaussian 03 results with a) 6-311G, b) SDD, c) TZVP; VASP results for the molecule d) in the gas phase and e) on graphite (first 3 unoccupied orbitals).

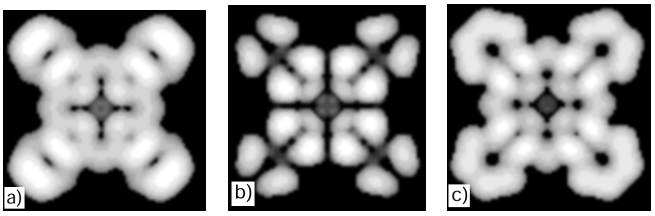


FIG. 13: Occupied orbitals of CuPc as far as a) 2 eV and b) 1.5 eV (2 orbitals) below the HOMO, c) unoccupied orbitals up to 2 eV above the LUMO, calculated with B3LYP/TZVP.

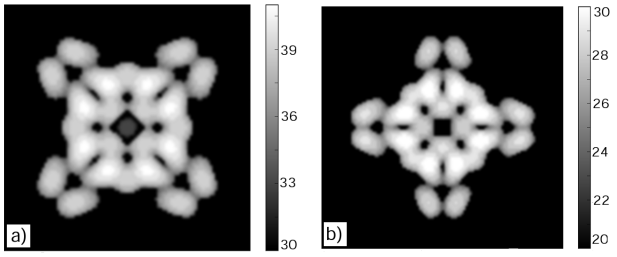


FIG. 14: LUMO of a) copper phthalocyanine and b) phthalocyanine, calculated with B3LYP/TZVP. Note the different range of the gray scale. With the same scaling, panel (a) would be much brighter.

STM images, a specific influence of the central copper atom on the appearance of the STM image is not discernible (see Fig. 14). The orbitals chosen for the simulation are mainly centered on the phthalocyanine ligand. Small protrusions in the center of the molecule can be seen in the metal complex only, but they are insignificant compared to the brightly accentuated pyrrole rings of the ligand. The main difference between the phthalocyanine ligand and a metal phthalocyanine complex is the higher density of states and with it higher overall brightness of the metal complex (note that in Fig. 14 we chose the same contrast in both panels; If the gray scaling was the same, Fig. 14a would be much brighter than Fig. 14b).

For the oligopyridine 3,3'-BTP, more orbitals are available in the same energy range, so the number of orbitals used in the simulation is higher. STM images of 3,3'-BTP generally are of twofold symmetry. Images based on unoccupied orbitals differ in structural details like position and number of nodal planes from images based on occupied orbitals. The shape of the simulated STM image is the same in both cases. Using occupied orbitals results in images with maximum brightness on the phenyl ring (Fig. 15). Using unoccupied orbitals results in images where the pyrimidine group and the neighboring pyridine rings are emphasized (Fig. 16 b) and c)).

Another point of interest is the conformation of the adsorbed oligopyridine molecule. Depending on the force field used, calculated results for torsion angles between aromatic rings vary strongly. The surface conformation obtained with the Universal force field was used for DFT electronic optimizations of isolated molecules. In the surface conformation, pyridine ring B is considerably rotated out of the molecular plane and the part that protrudes above the rest of the molecule is displayed brighter in the simulated STM images. However, differences are rather small and even decrease when simulation parameters are adjusted to better represent experimental STM conditions (Fig. 15).

Different DFT methods and basis sets provide images similar in shape, but different in details such as brightness or size of single orbital lobes. The differences are caused by variations in orbital distribution in the fixed energy range according to the chosen basis set and DFT method. For copper phthalocyanine, this can be observed in the center of the molecule around the position of the copper atom (Fig. 12 a) – d)). For 3,3'-BTP, differences occur mainly in the representation of pyridine ring B (Fig. 15 a) – d)).

In order to assess the influence of the substrate on the STM images, an additional graphene layer under the molecule was used to model more realistically the surface situation. As DFT is known to underestimate the van der Waals interaction between aromatic systems [49] and therefore overestimates the distance between graphite surfaces and aromatic adsorbates [50], we based our STM simulations of adsorbed molecules on force field results: The adsorption structure of the copper phthalocyanine and the BTP molecules, respectively, on graphite was optimized with the Universal force field, then this conformation was used for DFT calculations that yielded the electronic information needed for the STM simulation. Upon inclusion of the graphene layer, additional orbitals mainly centered on the graphene layer appear

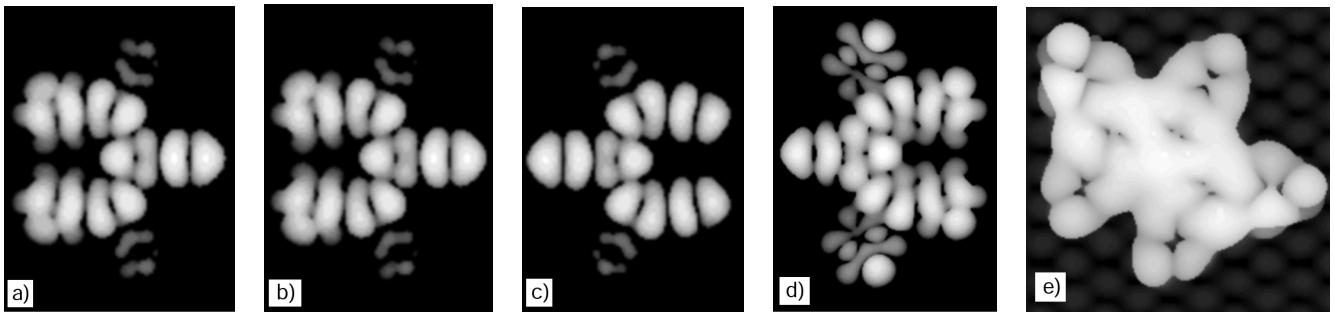


FIG. 15: Simulated STM images of 3,3'-BTP. Occupied orbitals as far as 0.3 eV below the HOMO were taken into account. Gaussian 03 results for a planar molecule in the gas phase with a) B3LYP/6-311G, b) B3LYP/SDD, c) B3LYP/TZVP. VASP results for the molecule d) in a planar gas phase structure and e) in a non-planar conformation on graphite with the configuration taken from an UFF optimization (unoccupied orbitals in the surface conformation up to 1.2 eV above the LUMO)

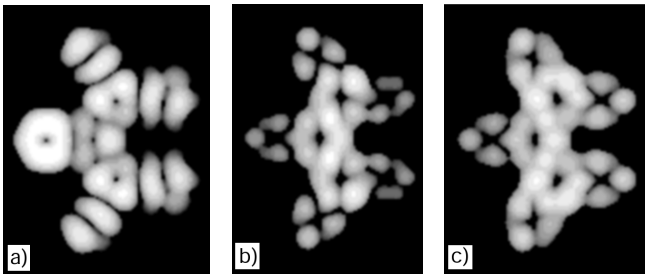


FIG. 16: a) Occupied orbitals of 3,3'-BTP as far as 0.5 eV below the HOMO, unoccupied orbitals up to b) 0.2 eV and c) 0.7 eV above the LUMO, calculated with B3LYP/TZVP

and a higher number of orbitals is available for comparable energy ranges. However, compared to the simulation of gas-phase molecules, significant differences can not be observed in our simulations (Fig. 12e, 15e). This confirms that for these physisorbed molecules the presence of the substrate hardly modifies their electronic structure. Therefore, the alterations induced by the presence of an additional graphene layer as a model for the substrate are probably too small to justify the increased computational effort required for the DFT calculations including the graphite substrate.

## IV. CONCLUSIONS

Different properties of oligopyridine-based surface template structures were studied with force field and DFT methods. Results obtained with the UFF, CVFF, Dreiding and Compass force fields were compared in order to to determine the force field best suited for the description of the oligopyridine surface structure.

Calculations of different model properties shows that the preferential choice of force field depends on the problem studied: Only UFF is able to yield appropriate torsion angles and biarylic C-C single bond lengths, whereas adsorption energies are least overestimated with Compass. Suitable torsional potentials can be obtained with both Compass and UFF, depending on the bipyridine isomer.

Our density functional perturbation theory calculations show that a planar arrangement of the 3,3'-BTP monomers within a free-standing monolayer is dominated by repulsive interactions. Indeed, the planarity of the 3,3'-BTP unit is hindering the formation of weak intermolecular interactions and the torsion angle between rings B and C is the key to the onset of attractive interactions within the monolayer.

3,3'-BTP surface structure calculations on graphite result in a hexagonal 19×19 surface unit cell. The lattice constant of this optimum cell is 45.96-46.78 Å, with a Compass adsorption energy of 428 kJ/mol per molecule. UFF suggests non-planar conformations of the adsorbed molecules with torsion angles smaller than in the gas phase. The structure possesses large cavities that can be used as a template for the adsorption of additional bipyridine or phthalocyanine. The template structure remains virtually unchanged upon adsorption of a guest molecule. Compass results for the adsorption energy are 416 kJ/mol for 3,3-BTP and 330 kJ/mol for phthalocyanine.

Phthalocyanine molecules can rotate within the cavities, with barriers ranging form 33.4 kJ/mol (Compass) to 54.8 kJ/mol (UFF). At room temperature, these barriers enable a rotational motion faster than the scanning process, so the geometry of the phthalocyanine molecule will not be resolved in STM images. As several local minima exist, the system is very sensitive towards slight alterations of the initial geometry.

Our STM simulations are based on DFT calculations carried out with VASP and Gaussian 03 (B3LYP) using 6-311G, SDD and TZVP basis sets. For the simulation, an energy range close to HOMO and LUMO should be used. The choice of basis set and DFT method can influence structural details, mainly when the number of orbitals in the given energy range varies strongly. The graphite substrate has only a minor influence on STM images. Adding metal atoms to the phthalocyanine ligand changes the brightness of the image, whereas an ad-

ditional graphene layer has no significant effect.

**Acknowledgments**

Financial support by the Deutsche Forschungsgemeinschaft (DFG) within SFB 569 is gratefully acknowledged. We thank our colleagues Chr. Meier and U. Ziener for useful discussions.

[1] Rosei, F.; Schunack, M.; Naitoh, Y.; Jiang, P.; Gourdon, A.; Lægsgaard, E.; Stensgaard, I.; Joachim, C.; Besenbacher, F. *Prog. Surf. Sci.* **2003**, *71*, 95.
[2] Lackinger, M.; Griessl, S.; Markert, T.; Jamitzky, F.; Heckl, W. M. *J. Phys. Chem. B* **2004**, *108*, 13652–13655.
[3] Boyen, H.-G.; Ziemann, P.; Wiedwald, U.; Ivanova, V.; Kolb, D. M.; Sakong, S.; Groß, A.; Romanyuk, A.; Büttner, M.; Oelhafen, P. *Nature Mater.* **2006**, *5*, 394.
[4] Meier, C.; Landfester, K.; Künzel, D.; Markert, T.; Groß, A.; Ziener, U. *Angew. Chem. Int. Ed.* **2008**, *47*, 3821.
[5] Meier, C.; Landfester, K.; Ziener, U. *J. Phys. Chem. C* **2008**, *112*, 15236–15240.
[6] Meier, C.; Ziener, U.; Landfester, K.; Weihrich, P. *J. Phys. Chem. B* **2005**, *109*, 21015.
[7] Ziener, U. *J. Phys. Chem. B* **2008**, *112*, 14698–14717.
[8] Ziener, U.; Lehn, J.-M.; Mourran, A.; Möller, M. *Chem. Eur. J.* **2002**, *8*, 951.
[9] Groß, A. *J. Comput. Theor. Nanosci.* **2008**, *5*, 894.
[10] Rappé, A. K.; Casewit, C. J.; Colwell, K. S.; Goddard, W. A.; Skiff, W. M. *J. Am. Chem. Soc.* **1992**, *114*, 10024.
[11] Sun, H. *J. Phys. Chem. B* **1998**, *102*, 7338.
[12] Mayo, S. L.; Olafson, B. D.; Goddard, W. A. *J. Phys. Chem.* **1990**, *94*, 8897.
[13] Dauber-Osguthorpe, P.; Roberts, V. A.; Osguthorpe, D. J.; Wolff, J.; Genest, M.; Hagler, A. T. *PROTEINS: Structure, Function, and Genetics* **1988**, *4*, 31.
[14] Gasteiger, J.; Masili, M. *Tetrahedron* **1980**, *36*, 3219.
[15] CPMD, Copyright IBM Corp 19902004, Copyright MPI für Festkörperforschung Stuttgart, 1997-2001.
[16] Perdew, J. P.; Burke, K.; Ernzerhof, M. *Phys. Rev. Lett.* **1996**, *77*, 3865.
[17] Hyla-Kryspin, I.; Haufe, G.; Grimme, S. *Chem. Eur. J.* **2004**, *10*, 3411.
[18] Vanderbilt, D. *Phys. Rev. B* **1990**, *41*, 7892.
[19] Billeter, S. R.; Curioni, A.; Andreoni, W. *Comput. Mat. Sci.* **2003**, *27*, 437.
[20] Benoit, D. M.; Sebastiani, D.; Parrinello, M. *Phys. Rev. Lett.* **2001**, *87*, 226401.
[21] Goedecker, S.; Teter, M.; Hutter, J. *Phys. Rev. B* **1996**, *54*, 1703.
[22] Hartwigsen, C.; Goedecker, S.; Hutter, J. *J. Phys. Rev. B* **1998**, *58*, 3641.
[23] Ludwig, C.; Strohmaier, R.; Petersen, J.; Gompf, B.; Eisenmenger, W. *J. Vac. Sci. Technol. B* **1994**, *12*, 1963.
[24] Lippel, P. H.; Wilson, R. J.; Miller, M. D.; Wöll, C.; Chiang, S. *Phys. Rev. Lett.* **1989**, *62*, 171.
[25] Gaussian 03, Revision D.01. Frisch, M. J.; Trucks, G. W.; Schlegel, H. B.; Scuseria, G. E.; Robb, M. A.; Cheeseman, J. R.; Montgomery, Jr., J. A.; Vreven, T.; Kudin, K. N.; Burant, J. C.; Millam, J. M.; Iyengar, S. S.; Tomasi, J.; Barone, V.; Mennucci, B.; Cossi, M.; Scalmani, G.; Rega, N.; Petersson, G. A.; Nakatsuji, H.; Hada, M.; Ehara, M.; Toyota, K.; Fukuda, R.; Hasegawa, J.; Ishida, M.; Nakajima, T.; Honda, Y.; Kitao, O.; Nakai, H.; Klene, M.; Li, X.; Knox, J. E.; Hratchian, H. P.; Cross, J. B.; Bakken, V.; Adamo, C.; Jaramillo, J.; Gomperts, R.; Stratmann, R. E.; Yazyev, O.; Austin, A. J.; Cammi, R.; Pomelli, C.; Ochterski, J. W.; Ayala, P. Y.; Morokuma, K.; Voth, G. A.; Salvador, P.; Dannenberg, J. J.; Zakrzewski, V. G.; Dapprich, S.; Daniels, A. D.; Strain, M. C.; Farkas, O.; Malick, D. K.; Rabuck, A. D.; Raghavachari, K.; Foresman, J. B.; Ortiz, J. V.; Cui, Q.; Baboul, A. G.; Clifford, S.; Cioslowski, J.; Stefanov, B. B.; Liu, G.; Liashenko, A.; Piskorz, P.; Komaromi, I.; Martin, R. L.; Fox, D. J.; Keith, T.; Al-Laham, M. A.; Peng, C. Y.; Nanayakkara, A.; Challacombe, M.; Gill, P. M. W.; Johnson, B.; Chen, W.; Wong, M. W.; Gonzalez, C.; Pople, J. A. Gaussian, Inc., Wallingford, CT, **2004**.
[26] Becke, A. D. *J. Chem. Phys.* **1993**, *98*, 5648.
[27] Kresse, G.; Furthmüller, J. *Phys. Rev. B* **1996**, *54*, 11169.
[28] Blöchl, P. E. *Phys. Rev. B* **1994**, *50*, 17953.
[29] Kresse, G.; Joubert, D. *Phys. Rev. B* **1999**, *59*, 1758.
[30] Tersoff, J.; Hamann, D. R. *Phys. Rev. B* **1985**, *31*, 805.
[31] Almenningen, A.; Bastiansen, O.; Gundersen, S.; Samdal, S. *Acta Chemica Scandinavica* **1989**, *43*, 932.
[32] Mata, F.; Quitana, M. J.; Sørensen, G. O. *J. Mol. Struct.* **1977**, *42*, 1.
[33] Almenningen, A.; Bastiansen, O. *Kgl. Norske Vid. Selsk. Skr.* **1958**, *4*.
[34] Schäfer, A.; Huber, C.; Ahlrichs, R. *J. Chem. Phys.* **1994**, *100*, 5829.
[35] Corongiu, G.; Nava, P. *International Journal of Quantum Chemistry* **2003**, *93*, 395.
[36] Pérez-Jiménez, A. J.; Sancho-García, J. C.; Pérez-Jordá, J. M. *J. Chem. Phys.* **2005**, *123*, 134309.
[37] Zacharia, R.; Ulbricht, H.; Hertel, T. *Phys. Rev. B* **2004**, *69*, 155406.
[38] Arnett, E. M.; Hutchinson, B. J.; Healy, M. H. *J. Am. Chem. Soc.* **1988**, *110*, 5255.
[39] Mignon, P.; Loverix, S.; De Proft, F.; Geerlings, P. *J. Phys. Chem. A* **2004**, *108*, 6038.
[40] Leach, A. R. *Molecular Modelling: Principles and Applications;* Pearson: Harlow, 2nd ed., 2001.
[41] Benoit, D. M.; Coulbeck, E.; Eames, J.; Motevalli, M. *Tetrahedron: Asymmetry* **2008**, *19*, 1068.
[42] Hartmann, M.; Wetmore, S. D.; Radom, L. *J. Phys. Chem. A* **2001**, *105*, 4470.
[43] McLean, A. D.; Chandler, G. S. *J. Chem. Phys.* **1980**, *72*, 5639.
[44] Dunning Jr., T. H.; Hay, P. J. In *Modern Theoretical Chemistry, Vol. 3*; Schaefer III, H. F., Ed.; Plenum: New York, 1976; pages 1–28.

[45] Dolg, M.; Wedig, U.; Stoll, H.; Preuss, H. *J. Chem. Phys.* **1987**, *86*, 866.
[46] Fuentealba, P.; v. Szentpály, L.; Stoll, H.; Fraschio, F. X.; Preuss, H. *J. Mol. Struct. (THEOCHEM)* **1983**, *93*, 213.
[47] Nilson, K.; Åhlund, J.; Brena, B.; Göthelid, E.; Schiessling, J.; Mårtensson, N.; Puglia, C. *J. Chem. Phys.* **2007**, *127*, 114702.
[48] Moors, M.; Krupski, A.; Degen, S.; Kralj, M.; Becker, C.; Wandelt, K. *Appl. Surf. Sci.* **2008**, *254*, 4251 – 4257.
[49] Kučera, J.; Groß, A. *Langmuir* **2008**, *24*, 13985.
[50] Ortmann, F.; Schmidt, W. G.; Bechstedt, F. *Phys. Rev. Lett.* **2005**, *95*, 186101.